Revealing the influence of Mo addition on interphase precipitation in Ti-bearing low carbon steels

Dong, Haokai; Chen, Hao; Riyahi khorasgani, Ahmadreza; Zhang, Boning; Zhang, Yongjie; Wang, Zhenqiang; Zhou, Xiaosheng; Wang, Wei; van der Zwaag, Sybrand; More Authors

DOI
10.1016/j.actamat.2021.117475

Publication date
2022

Document Version
Final published version

Published in
Acta Materialia

Acta Materialia 223 (2022) 117475

Contents lists available at ScienceDirect

Acta Materialia

journal homepage: www.elsevier.com/locate/actamat

Full length article

Revealing the influence of Mo addition on interphase precipitation in Ti-bearing low carbon steels

Haokai Dong[a,b], Hao Chen[a,*], Ahmadreza Riyahi khorasgani[c], Boning Zhang[a], Yongjie Zhang[d], Zhenqiang Wang[e], Xiaosheng Zhou[a], Wei Wang[f], Huanrong Wang[f], Tong Li[c], Zhigang Yang[a], Sybrand van der Zwaag[a,g]

[a] Key Laboratory of Advanced Materials of Ministry of Education, School of Materials Science and Engineering, Tsinghua University, Beijing 100084, China
[b] National Engineering Research Center of Near-net-shape Forming for Metallic Materials, South China University of Technology, Guangzhou 510641, China
[c] Institute for Materials, Ruhr-Universität Bochum, Universitätsstraße 150, Bochum 44801, Germany
[d] Institute for Materials Research, Tohoku University, Aoba-ku, Sendai, Miyagi 980-8577, Japan
[e] Key Laboratory of Superlight Materials and Surface Technology, Ministry of Education College of Material Science and Chemical Engineering, Harbin Engineering University, Harbin 150001, China
[f] Department of Hot Rolled Strip, Baosteel Research Institute, Shanghai 201900, China
[g] Faculty of Aerospace Engineering, Delft University of Technology, Delft, The Netherlands

ARTICLE INFO

Article history:
Received 2 July 2020
Revised 15 September 2021
Accepted 8 November 2021
Available online 10 November 2021

Keywords:
Interphase precipitation
(Ti, Mo)C
Carbide nucleation
Coarsening resistance
Interfacial energy
Trans-interface diffusivity

ABSTRACT

Mo is widely used as an effective microalloying element to improve mechanical performance of interphase precipitation steels, but the precise role of Mo in interphase precipitation behavior is not fully understood. In this contribution, interphase precipitation behavior in a series of Ti-Mo-bearing low carbon steels is systematically studied, and the role of Mo in interphase precipitates and its coarsening behavior is revisited. It is found that (Ti, Mo)C precipitates instead of TiC are formed in the Mo-containing alloys, and the average site fraction of Mo in (Ti, Mo)C is almost independent of the bulk Mo content. Moreover, the number density of interphase precipitates can be substantially enhanced by a minor addition of Mo, albeit it does not further rise with increasing the bulk Mo content. This is because the Mo fraction in (Ti, Mo)C rather than the bulk Mo content governs the driving force for precipitation nucleation and the interfacial energy of the (Ti, Mo)C/α and (Ti, Mo)C/γ interfaces. In addition to the reduced interfacial energy, decrease of Ti trans-interface diffusivity has been identified as another key reason for the enhanced carbide coarsening resistance in Mo-containing alloys.

1. Introduction

To satisfy the increasing demand for energy-saving and emission-reduction, various high-strength low-alloy (HSLA) steels have been developed in the automotive industry. However, the conventional HSLA steels with the multiphase microstructures are often prone to stress-concentration during loading, thereby deteriorating the local elongation. About two decades ago, a Ti-Mo-bearing hot rolled steel [1,2] that possesses a high density of nano-sized carbides orderly distributed in the ferritic matrix was developed, which drew extensive attention due to its superior strength and excellent stretch-flangeability. Nano-sized carbides in the Ti-Mo-bearing steels [3,4] was repeatedly formed at the migrating interfaces during the austenite (γ) to ferrite (α) transformations, which is so-called interphase precipitation. Similar phenomenon has also been observed in many other microalloyed steels (e.g. Nb [5], Nb-Ti [6], Ti-V [7], V [8]).

Mo is an important element in interphase precipitation steels as it has been found to play a critical role in number density, size and distribution of interphase precipitated carbides. Substantial efforts were made to investigate the effects of Mo addition on interphase precipitation behavior in the Ti-bearing low carbon steels because of their great industrial relevance [8–16]. The typical alloy composition used are 0.2Ti and 0.1Ti-0.2Mo with a fixed base composition 0.05C-1.5Mn-0.2Si in mass%. It has been experimentally confirmed that Mo can partially replace Ti atoms in TiC to form a complex (Ti, Mo)C, which could substantially enhance the number density of carbide and reduce the carbide size [1,14]. Using first-principles calculations, Jang et al. [17] claimed that Mo partitioning into TiC could reduce interfacial energy of the carbide/matrix interface, which assists the nucleation process, but they also pointed out that Mo partitioning into TiC could decreases

* Corresponding author.
E-mail address: hao.chen@mail.tsinghua.edu.cn (H. Chen).

https://doi.org/10.1016/j.actamat.2021.117475
1359-6454/

Table 1
Chemical compositions (mass%) and Ae_3 temperatures (°C) for the alloys used in this study.

Alloy	C	Si	Mn	N	Ti	Mo	Fe	Ortho-A_{e3}	Para-A_{e3}	NPLE/PLE
0Mo	0.048	0.22	1.48	0.0027	0.092	–	Bal.	839	820	785
0.1Mo	0.049	0.19	1.49	0.0024	0.105	0.096	Bal.	841	822	786
0.2Mo	0.050	0.21	1.46	0.0027	0.102	0.196	Bal.	843	824	787
0.3Mo	0.043	0.19	1.50	0.0029	0.098	0.285	Bal.	845	826	788

the nucleation driving force by increasing the formation energy of carbides. Therefore, Mo plays a complex role in carbide nucleation. For the Ti-Mo-containing steels, many studies [9,15,16,18] have showed that Mo contents in (Ti, Mo)C are much higher than the equilibrium values predicated by Thermo-Calc and the measured compositional ratio of Mo/(Ti+Mo) are unexpectedly close, which indicates that there may exist a critical Mo composition in (Ti, Mo)C that corresponds to the minimum barrier for carbide nucleation. Nevertheless, a quantitative analysis of Mo effects on nucleation barrier and thereby nucleation rate is still not available.

Mo addition was also found to retard the carbide coarsening. The role of Mo in coarsening kinetics of carbides has been comparatively studied in the two aforementioned steels (i.e. 0.2Ti and 0.1Ti-0.2Mo in mass%) [14,17,19]. There have been two mechanisms proposed to explain the slower coarsening rate in the 0.1Ti-0.2Mo steel. (i) A lower amount of remaining Ti solutes in the matrix due to the lower designed bulk Ti content [20]. (ii) A smaller interfacial energy of the (Ti, Mo)C/matrix interface due to the decreased misfit strain by refining the carbide lattice constant [17]. Recently, two model alloys with the same bulk Ti content (i.e. 0.1Ti and 0.1Ti-0.2Mo in mass%) have been studied by Wang et al. [18] through the small-angle neutron scattering (SANS) technique. They concluded that Mo addition barely retards the global growth and coarsening of (Ti, Mo)C, which contradicts with the previous observations [14,17,20].

In fact, carbide coarsening should not only be controlled by interfacial energy but also by solute diffusion across the carbide/matrix interface. For simple MC precipitates, solute diffusivity (e.g. Ti) near the carbide/matrix interface is usually assumed to be the bulk diffusivity, while this condition could be different once the impurity atom such as Mo partitions into TiC, as the interaction between Ti and Mo may alter Ti diffusivity across the carbide/matrix interface. Unfortunately, this issue has not been clarified yet as it is challenging to determine the trans-interface diffusivity of solute by experiments.

In this study, we aim to revisit the physical origin of Mo effects on interphase precipitation behavior in Ti-bearing low carbon steels. The effects of Mo addition on the nucleation of interphase precipitates are quantified by atom probe and high-resolution TEM, which is also rationalized by theoretical calculations. First-principle calculations are performed to investigate the effect of Mo on Ti diffusivity across the (Ti, Mo)C/matrix interface, and its contribution to coarsening resistance of (Ti, Mo)C is discussed.

2. Experimental and simulation

2.1. Experimental

A series of Fe-0.05C-1.5Mn-0.2Si-0.1Ti-based (mass%) alloys with different amounts of Mo addition were used in the present work. For simplicity, they are referred as 0Mo, 0.1Mo, 0.2Mo and 0.3Mo alloys hereafter. The chemical compositions and characteristic temperatures are listed in Table 1. All the temperatures were calculated by Thermo-Calc with TCFE9 database. The steels were fabricated by vacuum induction melting and then cast into ingots with dimensions of 220 × 240 × 250 mm^3. After homogenization at 1250 °C for 2 h, the ingots were hot-rolled to the plates with 7.5 mm thickness followed by air cooling. A Bahr DIL805A/D dilatometer equipped with a laser diameter detector was used for the heat treatment. The specimens were machined into standard cylindrical rods (4 mm in diameter and 10 mm in length) with the cylinder axis along the rolling direction. They were austenitized at 1200 °C for 3 min to dissolve any pre-existing carbides. The nominal γ grain size for each alloy was measured to be 100 ± 15 μm. Such small difference is expected to have a negligible effect on subsequent α transformation. After austenitization, the specimens were cooled to 660 °C with a cooling rate of 20 °C/s and isothermally held for 30 s to 7.2 ks, followed by helium gas quenching. In order to examine the effect of Mo addition on carbide coarsening, the as-quenched specimens were reheated to 660 °C and aged for 16 h in a separate furnace.

Transformed specimens for optical microscopy were polished and etched by 4% nital. Volume fractions of ferrite were quantified by point counting method, and final ferrite grain size was measured by linear intercept method. TEM observation (FEI TecnaiG20, operated at 300 kV), which allows large inclination angle (± 30°) for specimen holder, was carried out to characterize the interphase precipitation. TEM samples were produced by cutting slices from the dilatometer specimens and were mechanically thinned to 50 μm on SiC papers. Then, the thin-foil specimens were twin-jet electropolished at 20 V in a solution of 10% perchloric acid and 90% ethanol at -30 °C. The coarsened carbides in the aged specimens were extracted by carbon replica method. Their crystal structure, lattice constant and chemical composition are identified by high resolution TEM (HR-TEM) combined with nanobeam EDS (FEI TecnaiF20, operated at 200 kV).

Needle-shaped APT specimens were prepared by using a FEI Helios G4 CX focused ion beam (FIB) / scanning electron microscope. APT specimens were characterized by Cameca LEAP 5000 XR instrument with a detection efficiency of ~ 52%. The analyses were conducted in the voltage pulsing mode at a specimen temperature of 70 K with a target evaporation rate of 4 ions per 1000 pulses, pulse fraction of 20%, and a pulse rate of 125 kHz. The APT data was reconstructed and analyzed using the commercial IVAS 3.8.2 software. MC precipitates (M=Ti, Mo) in the transformed specimens were quantified by cluster analysis through maximum separation method [21]. 0.85 nm and 10 atoms were selected to be the values for d_{max} and N_{min}, respectively, based on the nearest neighbor distribution and cluster size distribution. Considering that the artefact in APT analysis is more significant for C compared to the substitutional elements [22], only metallic elements were taken as the solute atoms for cluster analysis in this study. Then, the dispersion of interphase precipitation is quantified by number density and particle size. The number density of MC (ρ) can be simply estimated by dividing the number of detected clusters by the volume of the measured needle specimen. The cluster volume was calculated from the number of Ti+Mo atoms in each MC cluster, taking into consideration the detection efficiency of APT and the lattice constant of TiC (0.433 nm [23]). The radius of each MC (r) was obtained by assuming the precipitates to have a spherical shape.

2.2. Simulation

In order to understand the role of Mo in growth (or coarsening) behavior of multicomponent carbide, first-principles calculations based on the density functional theory were carried out. All calculations were performed using the Vienna Ab-initio Package (VASP) [24]. The projector-augmented wave (PAW) method [25,26] was used to describe ion-electron interactions, while the generalized gradient approximation (GGA) [27] parameterized by Perdew-Burke-Ernzerhof (PBE) [28] were used for electron exchange and correlation. A plane wave cut-off energy of 450 eV and first-order Mehthfessel-Paxton scheme [29] with a 0.1 eV smearing width were adopted. During the structural relaxation, both atomic positions and lattice were relaxed until the residual force on any atom was less than 0.01 eV/Å. The diffusion energy of Ti across the interface was calculated by using the climbing-image nudged-elastic-band method (CINEB) [30], with the convergence criterion for atomic forces set at 0.02 eV/Å.

3. Results

3.1. Microstructures and transformation kinetics

Fig. 1 shows the optical microstructures of the specimens transformed at 660 °C for 300 s and 3.6 ks, respectively. Allotriomorphic α (AF) is the sole transformation product for all specimens. The number and size of α grains at the early transformation stage (300 s) tend to decrease with increasing Mo content, which suggests that addition of Mo can suppress α nucleation. For the 0.3Mo alloy, the $\gamma \rightarrow \alpha$ transformation does not start even after 300 s (Fig. 1**(g)**), while the other specimens are almost fully transformed into AF after holding for 3.6 ks. Since the bulk compositional ratios in atom percent of C to Ti+Mo in the 0Mo (1:0.5) and 0.1Mo (1: 0.75) alloys exceed 1:1, a few C atoms will be enriched in γ even all Ti and Mo atoms are precipitated, thus resulting in a very small amount of martensite, as shown in Fig. 2**(b,d)**.

Fig. 2 shows the kinetics of isothermal $\gamma \rightarrow \alpha$ transformation at 660 °C. The solid lines are derived from the dilatation curves using the lever rule, and the dashed lines are obtained by fitting the measured fractions of interrupt specimens. It is found that Mo addition retards the ferrite formation severely, though the transformation kinetics from the dilatation curve is slightly faster than that determined by the metallographic method (Fig. 2). In the 0Mo alloy, the transformation stasis is reached at $\sim$ 0.8 ks, while addition of 0.3Mo postponed it to $\sim$ 4.7 ks. The α fractions predicted by the PE and NPLE/PLE models are plotted in Fig. 2. Only the curves of the 0.3Mo alloy are shown here due to the negligible difference between the studied alloys. The α fractions are obviously underestimated by both PE and NPLE models but are in good agreement with their counterparts that take C consumed by MC precipitation into account.

It has been well recognized that Mo addition can retard α formation kinetics by suppressing both nucleation and growth [31–33]. In this study, the α growth kinetics is of more interest since it can influence the interphase precipitation behavior as reported elsewhere [34–36]. Due to the irregular α morphology and relatively small grain size, it is hard to accurately derive the interface velocity ($v_{\alpha/\gamma}$) by following the traditional method, i.e. measuring the maximum half thickness of α as a function of reaction time. Thus, we chose to use Eq. (1) to estimate the average $v_{\alpha/\gamma}$ in the present work [37]:

$$df/dt = 3\left(1-f^2\right)\bar{R}^{-1}\, v_{\alpha/\gamma} arctanh^{(2/3)}(f) \quad (1)$$

where *df/dt* is the transformation rate, *f* is the transformed fraction, $\bar{R}$ is the average grain radius of α (46 μm in 0Mo, 52 μm in 0.1Mo, 75 μm in 0.2Mo, 71 μm in 0.3Mo). Fig. 3 shows the calculated $v_{\alpha/\gamma}$ as a function of α fraction for each alloy. It indicates that the average interface velocity (see insert) decreases with increasing Mo addition, which has been considered to be caused by solute drag effect of Mo segregation at the migrating α/γ interface [32,33].

3.2. Interphase precipitation

3.2.1. TEM observations

Fig. 4**(a–d)** shows the typical interphase-precipitated carbides in each specimen transformed at 660 °C for 3.6 ks. The planar morphology of interphase precipitation appears frequently in all the alloys. In some α grains, a seldomly reported morphology, called interrupted curved interphase precipitation having an irregular sheet spacing (ICIP), was occasionally detected, as arrowed in Fig. 4**(e)**. The intersheet spacing of ICIP is larger than the planar counterpart in general. Similar phenomena have also been observed in tungsten- and vanadium-containing steels [3]. Since carbide morphology is associated well with the structure of the migrating α/γ interface, Davenport et al. suggest that the formation of ICIP may be due to the irregular carbide nucleation on the growing ledges, i.e. nucleation at either the riser or on the terrace, or both (see Fig. 12(b) in [3]).

The measured planar intersheet spacing against bulk Mo content is plotted in Fig. 4**(f)**. The circles represent the intersheet spacing averaged from 10 to 15 measurements of individual α grains, and the solid squares represent the average intersheet spacing obtained from 4 to 5 α grains. It indicates that the intersheet spacing could vary from 10 to 25 nm but no clear correlation is obtained for the average intersheet spacing and the bulk Mo content.

3.2.2. APT analysis

APT analysis is performed to quantify the dispersion of MC interphase precipitates. Since occurrence of local magnification effects cannot be excluded especially for the clusters with a size of $<$ 1 nm, here we only choose the precipitates that have a relatively large size for compositional measurements, because the data from such kind of precipitates are more reliable than the nanoclusters due to the weaker artefacts. Fig. 5**(a)** shows the three-dimensional atom maps of Ti, Mo, C and Mn for the 0.3Mo specimen transformed at 660 °C for 3.6 ks. The localized enrichment of Ti, Mo and C atoms indicates that complex (Ti, Mo)C precipitates are formed. In contrast, the distribution of Mn atoms is uniform. Fig. 5**(b)** gives an enlarged map of one relatively large precipitate as highlighted by the dashed circle in Fig. 5**(a)**. According to the one-dimensional concentration profile measurements along the three mutually perpendicular directions, the co-precipitation of Ti, Mo and C atoms are clearly identified, and their total amount in the carbide is about 10 at.% balanced by Fe. This is a much lower percentage than the theoretical composition of B1-type MC precipitate (i.e. 50 at.% M and 50 at.% C). Similar results have also been reported in other types of nanoprecipitates [38,39], and were attributed to an artefact of APT measurement called local magnification effect [40]. Meanwhile, a hypo-stoichiometry of interstitial C content with respect to the substitutional carbide formers could be occasionally found, possibly because of the surface migration before evaporation [22] or the peak overlapping of Ti^{2+} and C_2^+ ions at 24 Da in mass spectra [41]. Furthermore, unlike the formation of compositional core-shell structure of (Ti, Mo)C in γ [19] or those in Ti, Mo, V-added low carbon steels [7], Ti and Mo atoms here are uniformly distributed across the (Ti, Mo)C irrespective of the measurement direction (Fig. 5**(b)**). Therefore, the following quantification of interphase precipitates dispersion in the Mo-containing alloys will be done by considering both Mo and Ti as the carbide formers.

Fig. 6 shows the three-dimensional Ti atom maps in α grains for each alloy transformed at 660 °C for 3.6 ks with superimposed

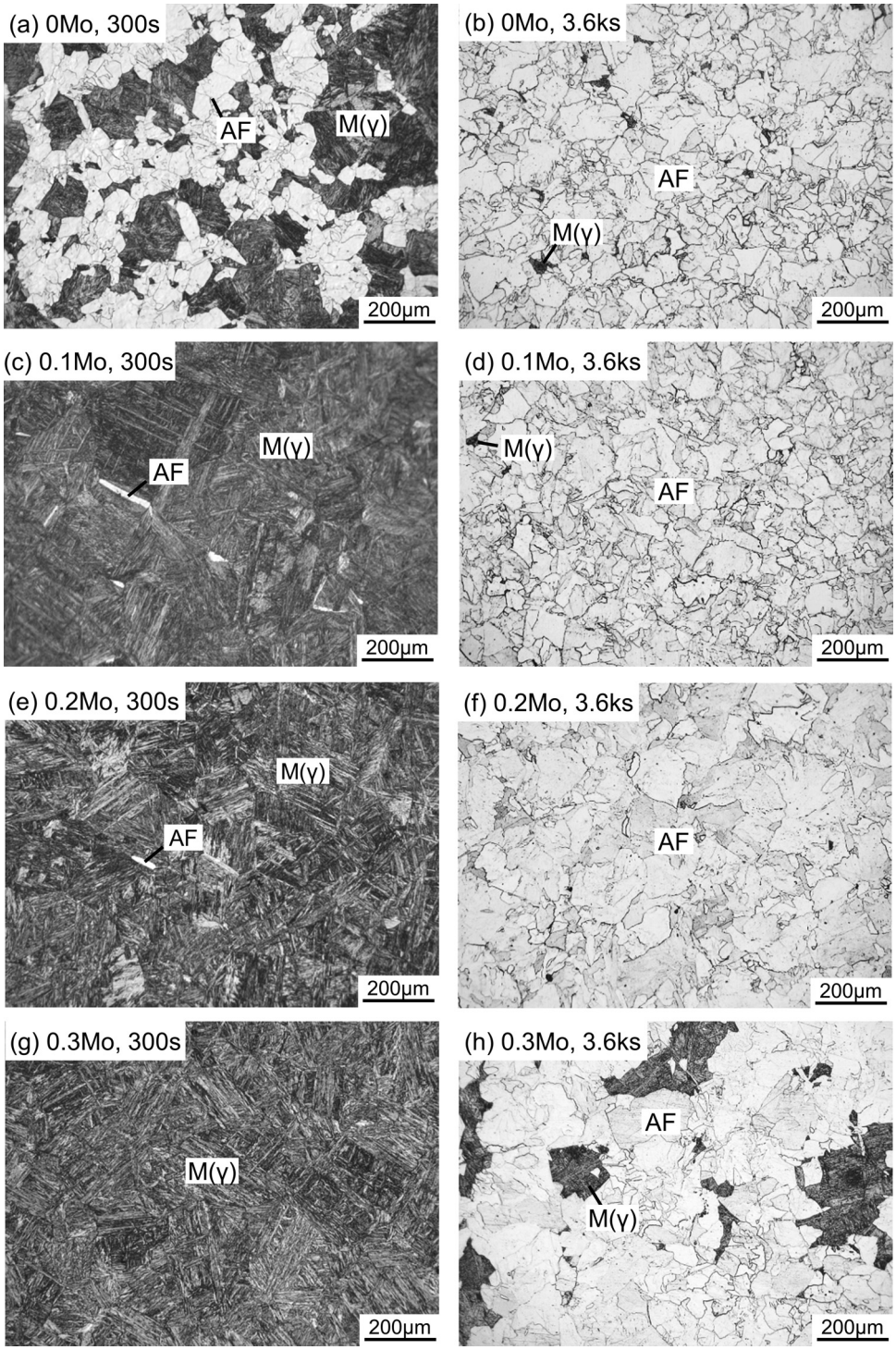

Fig. 1. Optical microstructures of (a,b) 0Mo, (c,d) 0.1Mo, (e,f) 0.2Mo and (g,h) 0.3Mo alloys transformed at 660 °C for (a,c,e,g) 300 s and (b,d,f,h) 3.6 ks. AF: allotriomorphic ferrite, M(γ): martensite.

1.5 at% Ti iso-concentration contours. Both random-like (Fig. 6**(a–c)**) and sheet-like dispersions (Fig. 6**(d)**) of MC precipitates can be captured. It should be noted that the sheet-like morphology does not always appear for interphase precipitation indeed, while the nanosized precipitates near the α/γ interface could be distributed randomly in many conditions, which has already been verified by a dedicated APT study [42]. Thus, the randomly-distributed carbides here are expected to be formed by the manner of interphase precipitation as well. APT characterization shows that the intersheet spacing of the 0.3Mo specimen measured in Fig. 6**(d)** ($\sim$ 9 nm) is close to the values obtained by TEM (Fig. 5**(f)**). Fig. 6**(e)** examines the distribution of interphase precipitates in the sheet plane. It is found that the MC precipitates are randomly distributed within the sheet plane, while the interparticle spacing estimated ($\sim$ 13 nm) is quite comparable to the intersheet spacing, implying that the interparticle spacing might be of equal importance to the intersheet spacing for precipitation hardening.

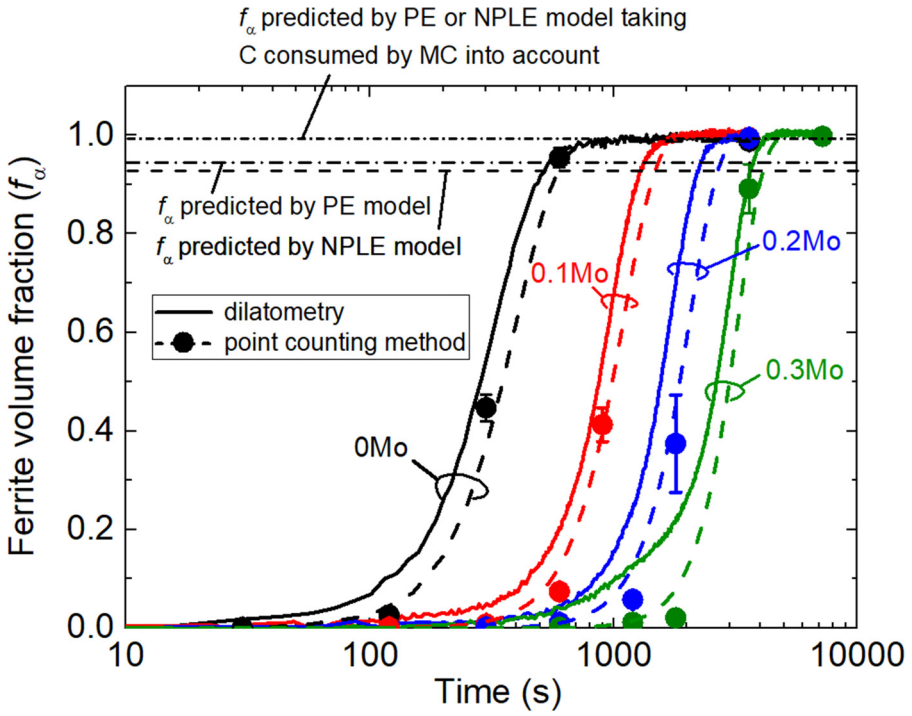

Fig. 2. Kinetics of ferrite transformation at 660 °C for each alloy.

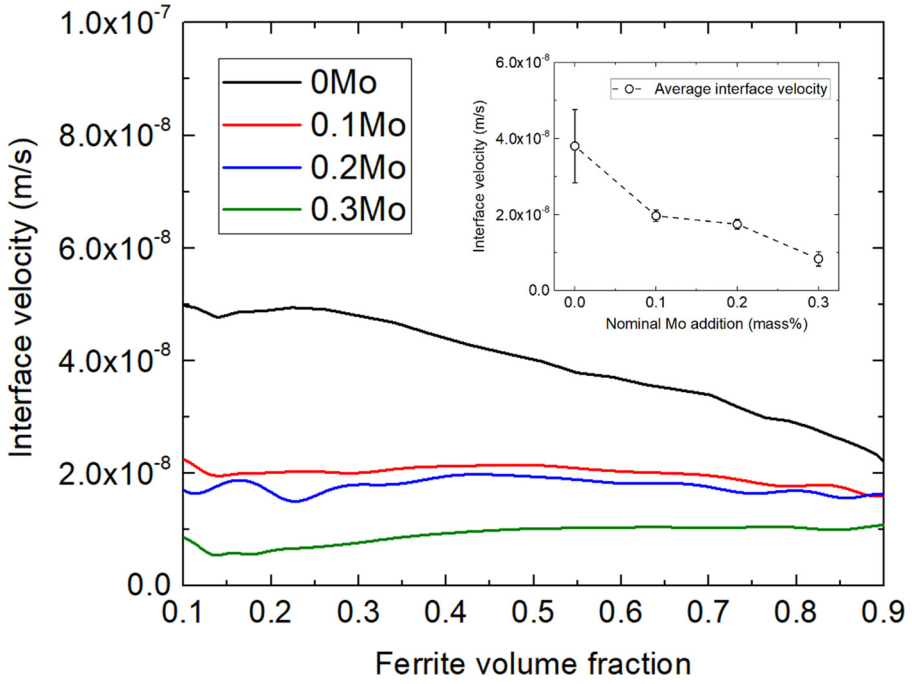

Fig. 3. The estimated interface velocity as a function of ferrite fraction for each alloy. Inset shows the variation of average interface velocity with nominal Mo addition.

Fig. 7 shows the number density (ρ), average carbide radius ($\bar{r}$), volume fraction of carbide (f_{MC}) and composition of (Ti, Mo)C in each alloy. According to Fig. 7**(a)**, the number density of MC precipitates increases about 1.7 times upon the addition of 0.1 mass% Mo, while a further increase in the bulk Mo content leads to a negligible change. The difference in average carbide radius between these alloys is minor. This could also be confirmed by the hardness and tensile tests as seen in Supplementary material Fig. S1 and S2. Both hardness and yield strength of the 0.1Mo steel are substantially higher than those of the 0Mo steel but are comparable with the 0.2Mo counterparts. In Fig. 7**(b)**, the volume fractions of carbide in the Mo-added alloys are more than 2 times larger than that in the 0Mo alloy, while all of them are much lower than their equilibrium values predicted by Thermo-Calc, which indicates that half or more than half of the carbide-forming elements must have remained in solid solution. Similar result was also obtained in the case of VC interphase precipitation [43]. The effect may be attributed to the Gibbs-Thomson effect as a result of the nanoscale particle size [44], i.e. an additional free energy that is inversely proportional to particle size should be added to MC precip-

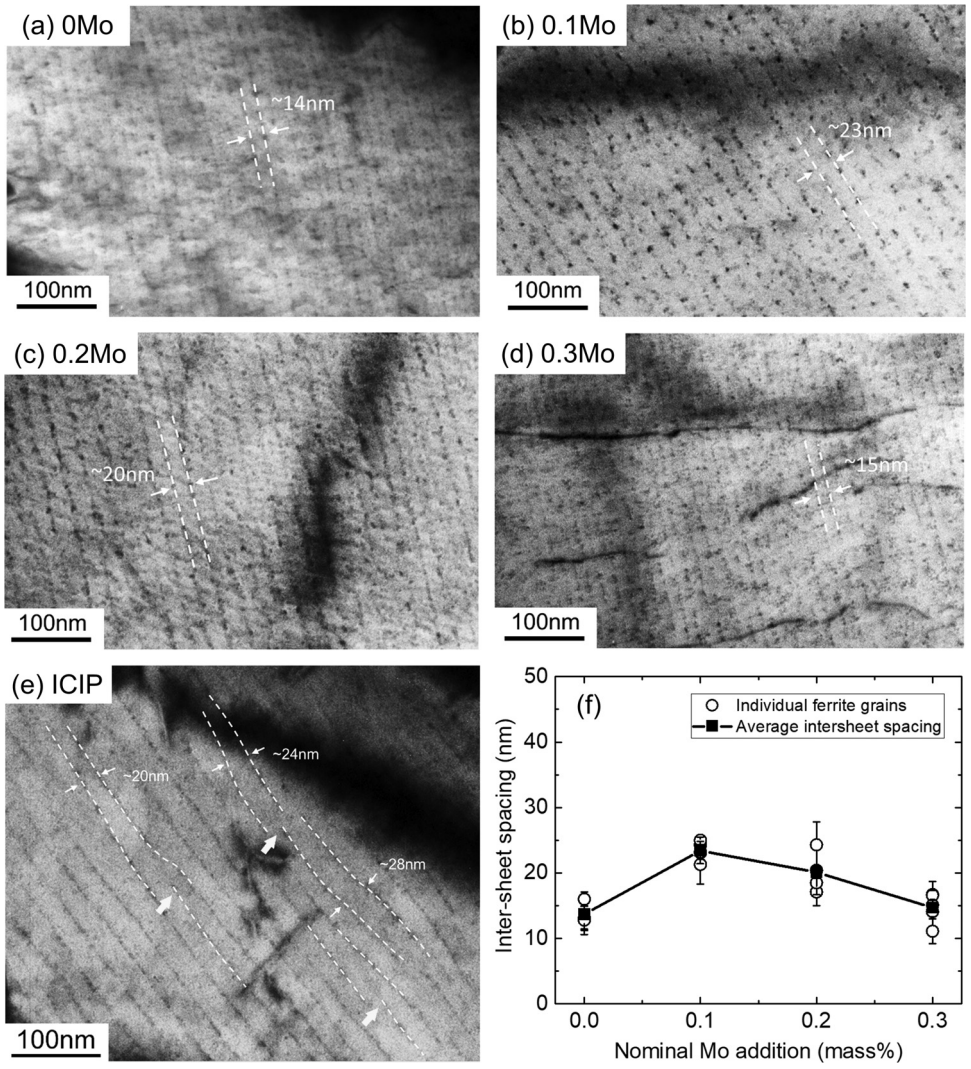

Fig. 4. TEM micrographs showing the typical morphology of interphase precipitation in (a) 0Mo, (b) 0.1Mo, (c) 0.2Mo and (d) 0.3Mo alloys transformed at 660 °C for 3.6 ks. (e) An example of the interrupted curved interphase precipitation (ICIP) with irregular intersheet spacing in the 0.2Mo specimen. The discontinuous carbide arrays are indicated by arrows. (f) Variations of intersheet spacing with nominal Mo addition.

itates when they are in equilibrium with α matrix. Fig. 7**(c)** shows the effect of Mo addition on MC composition. In order to mitigate the influence of local magnification effects, the ratio of detected Mo atoms against Mo+Ti atoms in the large precipitates (r>1 nm) are used to evaluate the composition. Interestingly, the average Mo content in (Ti, Mo)C is much higher than the equilibrium value but is almost independent of the bulk Mo content. The reason will be discussed in Section 4.2.

3.3. Carbide coarsening

Fig. 8 shows the TEM images of coarsened carbides in each alloy aged at 660 °C for 16 h. It is evident that the carbides in the 0Mo and 0.1Mo specimens are much coarser than those in the 0.2Mo and 0.3Mo alloys, which indicates that addition of more than 0.1 mass% Mo can enhance the carbide coarsening resistance substantially. This result is also consistent with the variation of the measured hardness as shown in **Supplementary material Fig. S1**. The carbide morphology exhibiting a shape of an oblate sphere can be clearly observed in the carbon replica. Due to the existence of projection error, it is hard to obtain the length of minor axes l_1 of carbides while the length of major axes l_2 is accessible by measuring the maximum distance between two points on the precipitate rim. To solve this problem, a reported aspect ratio of ~ 1.4 for (Ti, Mo)C transformed at 630–680 °C [11] is used in the present study. The length of minor axes and the carbide radius (r') defined as a radius of sphere having the same volume as that of an oblate spheroid can thus be expressed as $l_1 = l_2/1.4$ and $r' = (l_1 \cdot l_2^2)^{1/3}$, respectively. The mean radius is obtained by averaging r' of all the measured particles in the micrograph, as shown in Fig. 8 (right side). It reveals that the size of MC precipitates can be refined significantly by addition of more than 0.1 mass% Mo, and the distribution of particle radius appears to be narrower in the higher Mo-containing alloys, which is beneficial to lower the coarsening rate. The physical origin for Mo enhancing the coarsening resistance of carbide will be explained in Section 4.3.

4. Discussion

4.1. Effect of Mo addition on intersheet spacing

Intersheet spacing is a key microstructural feature for the interphase precipitation steels. The average intersheet spacing of MC precipitates changes slightly with the bulk Mo content (Fig. 5**(f)**), implying that addition of Mo might have a minor effect on the ledge height of the α/γ interface. According to the superledge

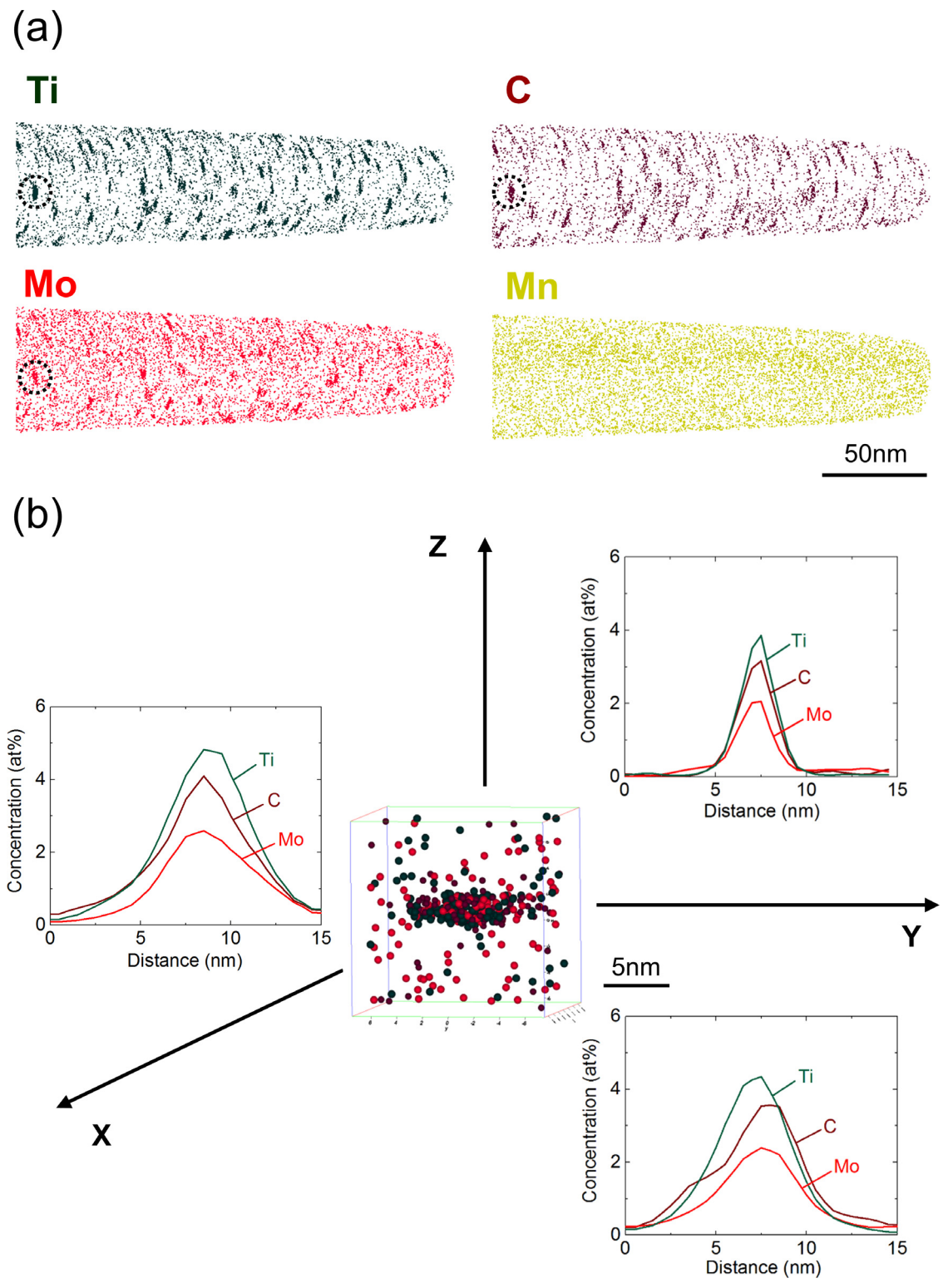

Fig. 5. (a) Three-dimensional atom maps of a ferrite grain in the 0.3Mo alloy transformed at 660 °C for 3.6 ks. (b) An atom map of one (Ti, Mo)C nanoprecipitate (as highlighted by a dashed circle in (a)) and one-dimensional concentration profiles along three perpendicular directions.

model [45], the critical ledge height, h^*, of the partially coherent interfaces correlates with the interfacial energy of the α/γ interface ($\sigma_{\alpha/\gamma}$) and the driving force for α nucleation ($\Delta G_m^{\gamma\to\alpha}$), i.e.

$$h^* = \sigma_{\alpha/\gamma} V_m / \Delta G_m^{\gamma\to\alpha} \tag{2}$$

Assuming that $\sigma_{\alpha/\gamma}$ is negligibly influenced by the minor Mo addition, the effect of Mo addition on h^* should be strongly linked to $\Delta G_m^{\gamma\to\alpha}$. For the evaluation of $\Delta G_m^{\gamma\to\alpha}$ in a multicomponent system, we firstly assume that the substitutional alloying elements (e.g. Mn, Ti, Mo) do not partition between the α and the parent γ, and C content in α (x_C^α) is in paraequilibrium with γ. Then, $\Delta G_m^{\gamma\to\alpha}$ can be calculated as

$$\Delta G_m^{\gamma\to\alpha} = \left(x_C^\alpha \mu_C^\gamma + x_{Mn}\mu_{Mn}^\gamma + x_{Ti}\mu_{Ti}^\gamma + x_{Mo}\mu_{Mo}^\gamma\right) - G^\alpha \tag{3}$$

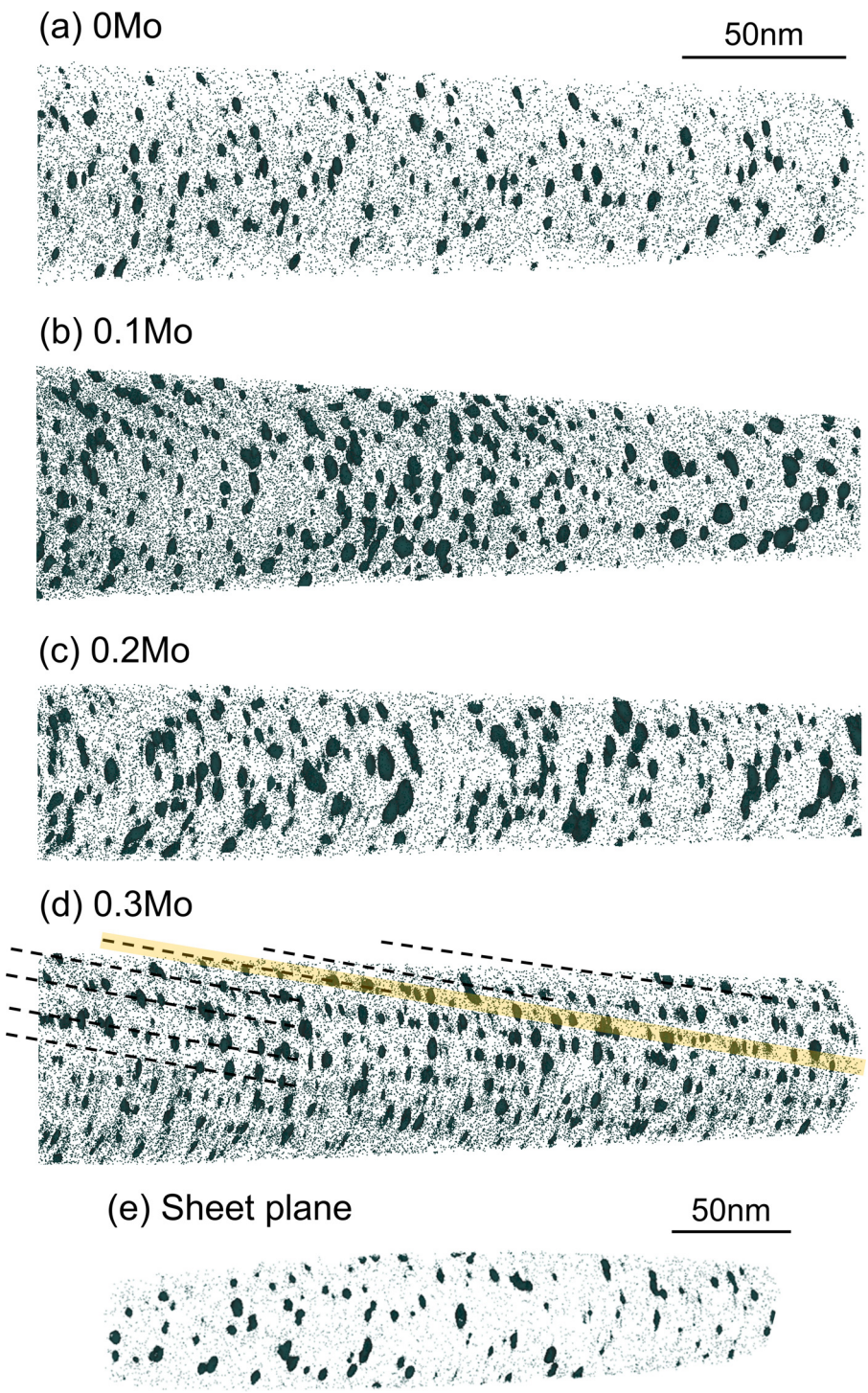

Fig. 6. Three-dimensional Ti atom maps superimposed by 1.5 at.% Ti isoconcentration surface of ferrite grains in (a) 0Mo, (b) 0.1Mo, (c) 0.2Mo and (d) 0.3Mo alloys transformed at 660 °C for 3.6 ks. (e) Distribution of interphase precipitates in one sheet plane extracted from the 0.3Mo alloy.

where x_i is the mole fraction of alloying elements in the bulk, μ_i^{γ} is the chemical potential of alloying elements in γ, G^{α} is the free energy of α that is in paraequilibrium with γ. By extracting the thermodynamic data from Thermo-Calc and substituting them into Eq. (3), the value of $\Delta G_m^{\gamma\rightarrow\alpha}$ is calculated to be 409–416 J/mol for the investigated alloys. Therefore, according to the superledge model, addition of Mo should have a marginal effect on the intersheet spacing, which is in good agreement with our experimental observation. Given the fact that interphase precipitation tends to occur at the non K-S interface rather than the K-S interface [42], 0.8 J/m^2 is assumed for $\sigma_{\alpha/\gamma}$ as a typical incoherent interface [46]. Then h^* is estimated to be $\sim$ 14 nm by Eq. (2), which is quite comparable with experiments.

4.2. Effect of Mo addition on the number density of precipitates

Compared with the intersheet spacing, it could be more important to elucidate the effect of Mo addition on number density as it determines the interparticle spacing in the slip plane and thus the mechanical properties. The number density of non-coarsened

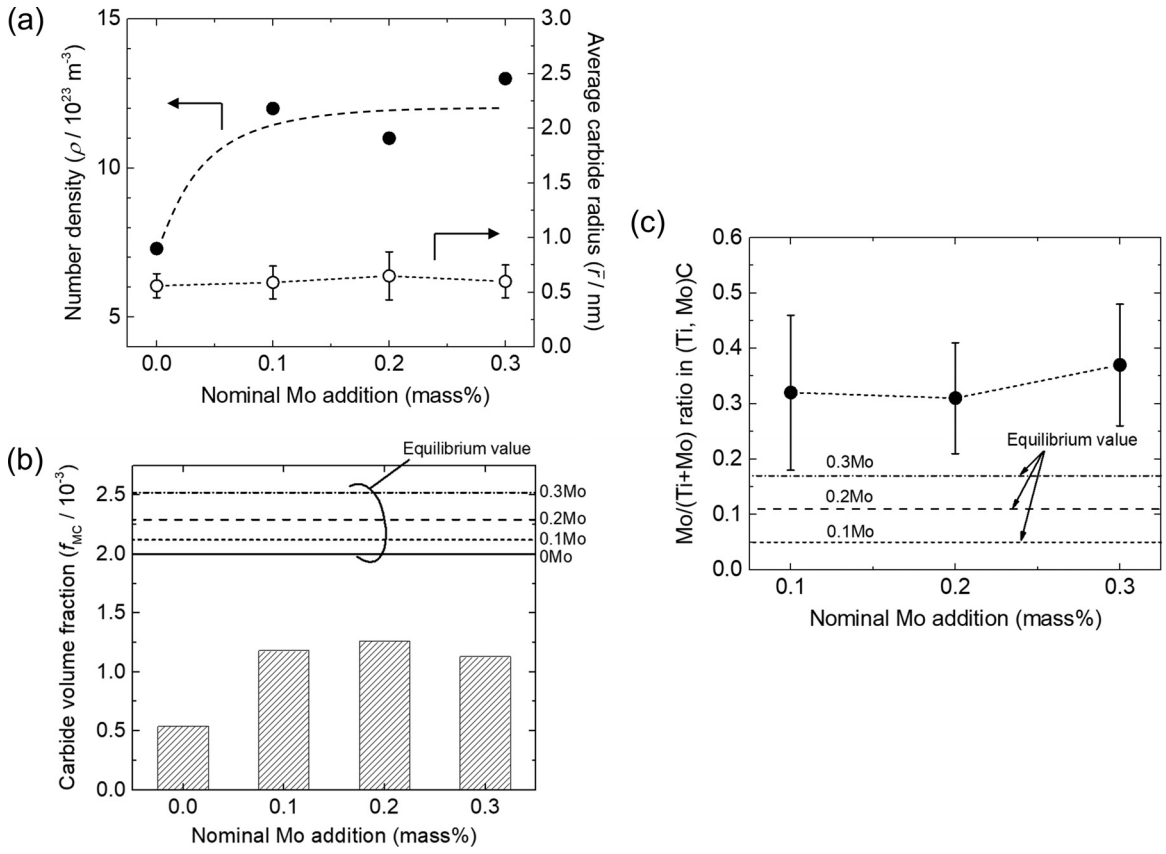

Fig. 7. (a) Number density, average carbide radius, (b) volume fraction and (c) average Mo content in (Ti, Mo)C as a function of nominal Mo addition in the alloys transformed at 660 °C for 3.6 ks.

precipitates is often controlled by nucleation rate. According to the classical nucleation theory [47], the nucleation rate of MC (I) at the migrating α/γ interface can be expressed as

$$I \propto N \cdot D_M^{int} \cdot exp\left(-\frac{\Delta G^*}{kT}\right) \tag{4}$$

where N is the number of nucleation sites per unit volume, D_M^{int} is the diffusivity of Ti or Mo along the α/γ interface, ΔG^* is the activation energy for MC nucleation at the interface, k is the Boltzmann constant and T is the temperature. In this study, nucleation sites of interphase precipitation are located at the migrating interface and the number should be proportional to the interface area per unit volume. Among the studied alloys, the value of N for the 0Mo alloy should be the largest as it has the smallest ferrite grain size. D_M^{int} is usually assumed to be the same magnitude as the grain boundary diffusivity for Fe [48]. Note that $N \cdot D_M^{int}$ for the Mo-added alloys is smaller than that of the 0Mo alloy while their number density of interphase precipitation is much higher. The emphasis in the subsequent analysis is thus placed on the effect of Mo on ΔG^*.

To derive the formula of ΔG^*, heterogeneous nucleation of MC interphase precipitation at the α/γ interface is considered. Fig. 9 shows the sketch of MC nucleation at the terrace plane of the α/γ interface. Assuming that the MC nuclei has a sphere shape with radius r, the associated free energy change of system can be written as

$$\Delta G = -V \cdot \Delta G_v + S_1\sigma_{\alpha/MC} + S_2\sigma_{\gamma/MC} - S_3\sigma_{\alpha/\gamma} + V\Delta G_s \tag{5}$$

where ΔG_v ($= \Delta G_m/V_m^{MC}$) is the driving force for MC nucleation, V_m^{MC} is the molar volume of precipitates ($\sim$ TiC $= 1.2 \times 10^{-5}$ m^3/mol), $\sigma_{\alpha/MC}$ and $\sigma_{\gamma/MC}$ are the interfacial energy of the α/MC and γ/MC interfaces, respectively, ΔG_s is the strain energy due to lattice misfit, $V = (4/3)\pi r^3$, $S_1 = S_2 = 2\pi r^2$, $S_3 = \pi r^2$. By differentiating Eq. (5) and ignoring the last term, we can obtain the critical nucleus size (r^*) and activation energy (ΔG^*) as

$$r^* = \frac{\left(2\sigma_{\alpha/MC} + 2\sigma_{\gamma/MC} - \sigma_{\alpha/\gamma}\right)V_m^{MC}}{2\Delta G_m} \tag{6}$$

$$\Delta G^* = \frac{\pi\left(2\sigma_{\alpha/MC} + 2\sigma_{\gamma/MC} - \sigma_{\alpha/\gamma}\right)^3}{12}\left(\frac{V_m^{MC}}{\Delta G_m}\right)^2 \tag{7}$$

Since incorporation of Mo in TiC have been confirmed to increase the formation energy of TiC (i.e. reducing the driving force for nucleation) but decrease the interfacial energy of the α/TiC interface [17], it can be realized that Mo addition can affect ΔG^* in a competitive manner according to Eq. (7), which should yield a critical condition that corresponds to the minimum ΔG^* and thereby the maximum I for interphase precipitation. In order to unravel the role of Mo in number density, we thus propose an alternative mechanism that considers the competitive effects of Mo partitioning into TiC on both ΔG_m and $\sigma_{\alpha,\,\gamma/MC}$.

Due to absence of thermodynamic information about the interface, the exact value of ΔG_m for interphase precipitation is still disputed. Here we assume that the interface migration proceeds in the NPLE mode where chemical potentials of Ti (μ_{Ti}), Mo (μ_{Mo}) and C (μ_C) in α and γ (with spike composition) at the interface are the same. Such assumption has been experimentally verified in an interphase precipitation study [49]. ΔG_m can be calculated as:

$$\Delta G_m = ((1-x)\mu_{Ti} + x\mu_{Mo} + \mu_C) - G_{(Ti_{1-x}Mo_x)C} \tag{8}$$

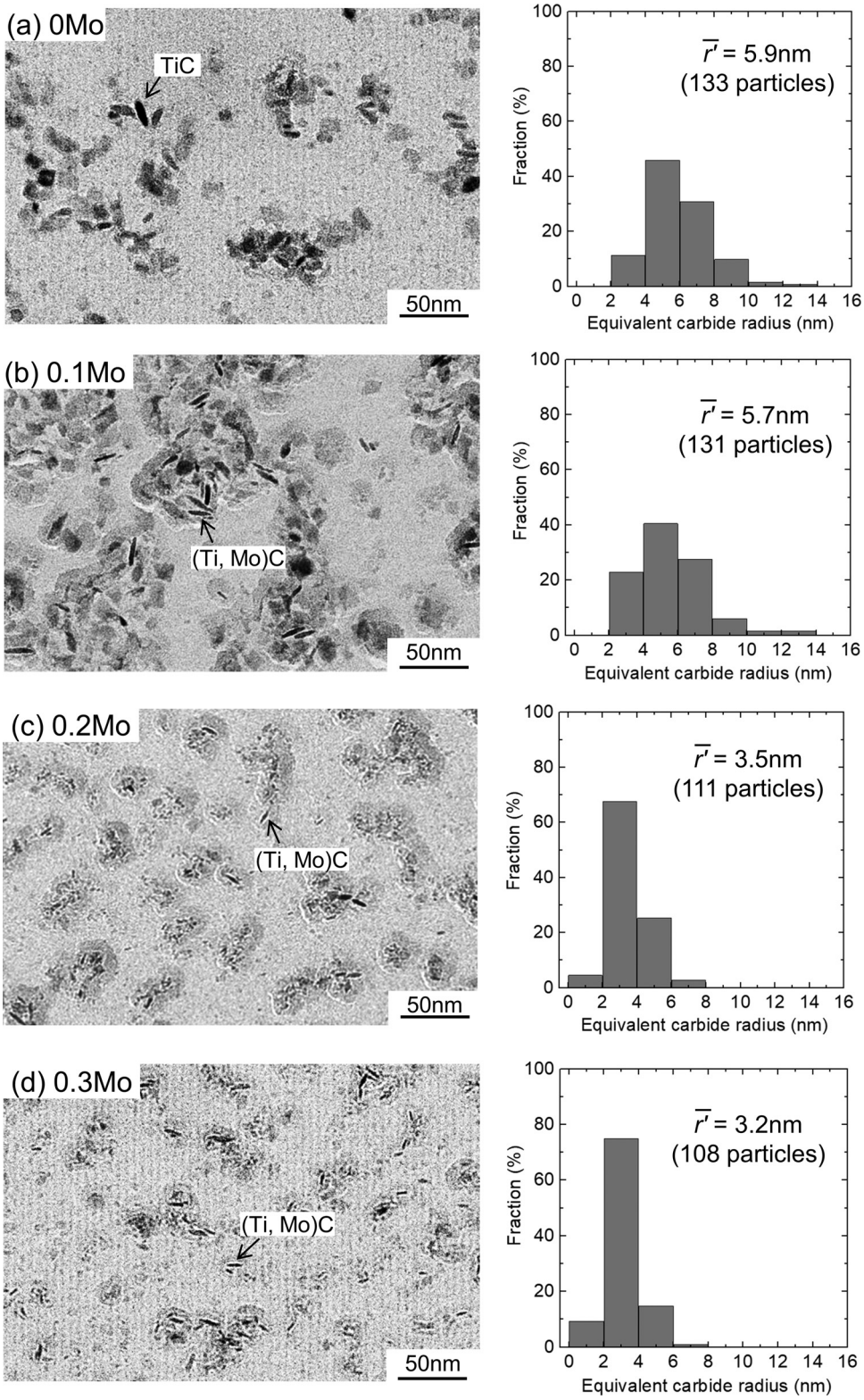

Fig. 8. Carbide distribution in carbon replicas and the corresponding statistical carbide radius for (a) 0Mo, (b) 0.1Mo, (c) 0.2Mo and (d) 0.3Mo alloys transformed at 660 °C for 16 h.

where x is the site fraction of Mo in carbide, $G_{(Ti_{1-x}Mo_x)C}$ is the free energy of carbide. Fig. 10**(a)** plots the calculated ΔG_m as a function of x by Thermo-Calc. It indicates that the ΔG_m decreases linearly with increasing x, while the bulk Mo content only has a marginal effect. The experimentally measured compositional range of (Ti, Mo)C is highlighted in the figure, and it shows that the ΔG_m for (Ti, Mo)C precipitation can be reduced by about one third of the pure TiC counterpart.

Then we consider the effect of Mo on interfacial energy of the α/MC and γ/MC interfaces. For the coherent (001) TiC/α and TiC/γ interfaces, the reported values of $\sigma_{\alpha/TiC}$ are in the range of 0.18 to 0.339 J/m^2 [17,50,51] and those of $\sigma_{\gamma/TiC}$ are $\sim$ 0.49 J/m^2 [52,54].

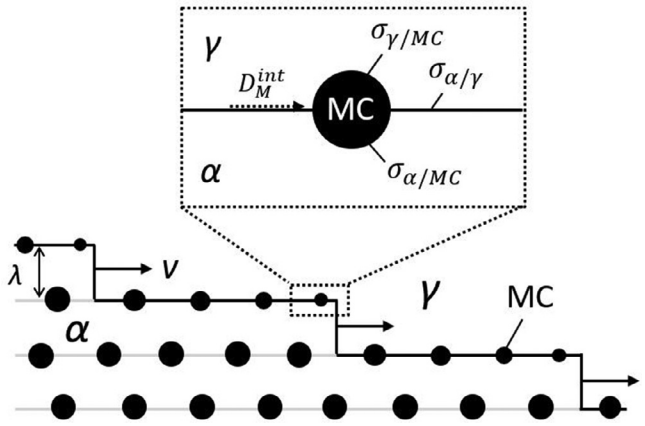

Fig. 9. Sketch of MC nucleation at the migrating α/γ interface under ledge mechanism.

By substituting these data and $\sigma_{\alpha/\gamma} = 0.8$ J/m^2 into Eq. (6), r^*, however, is estimated to be only 0.04 nm, which is unreasonably small. Actually, the interfacial energy consists of both chemical and structural components, and the latter arises from the lattice misfit between carbide and α matrix. The underestimation of r^* could be because $\sigma_{\alpha/MC}$ and $\sigma_{\gamma/TiC}$ derived by first-principles calculations only include the chemical contribution. Thus we take the values of $\sigma_{\alpha/TiC}$ and $\sigma_{\gamma/TiC}$ as 1.25 J/m^2 [53] and 2.38 J/m^2 [54] instead[1], where the former value is close to the reported ab initio calculation [55] that considers the contribution of lattice misfit.

Even though the first-principles calculations could reveal a quantitative correlation between chemical interfacial energy and Mo content in (Ti, Mo)C as seen in **Supplementary material Fig. S**3, the dependence of structural component of $\sigma_{\alpha/MC}$ and $\sigma_{\gamma/MC}$ on x remains unclear. We now propose two assumptions to simplify the analysis, i.e. assuming that (i) interfacial energy decreases linearly with x, e.g. $\sigma_{\alpha/MC} = 1.25 - kx$ (k is slope) and that (ii) the dependence of $\sigma_{\alpha/MC}$ and $\sigma_{\gamma/MC}$ on x is equal (i.e. k_α=k_γ). Fig. 10**(b)** shows the calculated ΔG^* as a function of x with different k values. As ΔG^* is similar for different alloys, only the calculation result of the 0.2Mo alloy are shown here. It is found that ΔG^* decreases monotonously with increasing x when $k = 2.0$, which suggests that incorporation of Mo into TiC can assist carbide nucleation but it fails to explain the measured compositional range of (Ti, Mo)C. The weak dependence of (Ti, Mo)C composition on the bulk Mo content (Fig. 7**(c)**) indicates that there may exist a critical composition x^* (in the nucleation stage) that corresponds to the minimum ΔG^*. Thus, a smaller k is needed to rationalize the observed results. By decreasing k, an energy valley point starts to appear and the corresponding x^* gradually reduces. The figure suggests that using $k = 1.43$ is the most appropriate to reproduce the experimental data, while a further decrease of k will increase the ΔG^* and make the valley point disappear. Fig. 10**(c)** plots the predicted x^* as a function of k. It reveals that x^* is sensitive to the choice of k and will become 0 (i.e. TiC) when k is reduced to 1.25.

Recently, some nanoclusters with a BCC structure have been captured by HR-TEM in Ti-Mo [15] and V-microalloyed [56] steels, suggesting that the embryo for interphase precipitation at the nucleation stage could be a metastable BCC phase rather than the equilibrium B1-type phase. Here we perform an approximate thermodynamic calculation for the nucleation of BCC-type nuclei. Similar to the case of B1-type carbide, ΔG_m for the BCC nucleus decreases with increasing x (Fig. 10**(d)**), while the absolute values are much lower than that for the B1-type carbide. It is interesting to note that such a low level of ΔG_m can still yield a reasonable value for r^* ($\sim$ 0.24 nm)[2] as the BCC nucleus keeps fully coherent with α matrix and thus should have quite low interfacial energy. Fig. 10**(e)** plots the calculated ΔG^* as a function of x. In this scenario, using $k = 0.58$ is the most appropriate to explain the measured composition of (Ti, Mo)C, while k values below 0.3 will lead to the MCs to form as a pure TiC embryo as shown in Fig. 10**(f)**. Furthermore, the fact that the derived value of ΔG^* in this case (1.15×10^{-20} J) is much lower than that for the nucleation of B1-type carbide (1.40×10^{-18} J) suggests that BCC-type phase is more energetically favorable than the B1-type phase to be a nucleus candidate, and might be responsible for the experimental observations [15].

Regardless of the nucleation scenario assumed, the fitting value of k should reflect the synergistic effects of Mo, including reduction of interfacial energy of both the α/MC and γ/MC interfaces by strengthening the atomic chemical bonding, mitigating the interface misfit strain and possibly promotion of vacancy formation [17] in carbides. Table 2 summarizes the measured Mo content in (Ti, Mo)C from other independent studies on Ti-Mo steels with bulk compositions close to the current 0.2Mo alloy. Interestingly, the Mo contents in (Ti, Mo)C obtained from the specimens transformed at 650–680 °C by different characterization techniques, are all around 30%. Such an unexpected coincidence indicates that the mechanism proposed in this study may be reasonable. In Ref. [1], the Mo content in (Ti, Mo)C formed during the continuous cooling was found to reach $\sim$ 46%, which could be ascribed to the value of ΔG_m that is temperature dependent.

In summary, Mo addition can increase the number density of MC by decreasing ΔG^*, while a further increase of the bulk Mo content can hardly increase the number density as Mo content in (Ti, Mo)C is almost independent on the bulk Mo content.

4.3. The role of Mo in carbide coarsening

Our TEM observations indicate that carbide coarsening can be significantly inhibited by addition of more than 0.1mass% Mo, which is in accordance with the findings in previous studies on the similar steels [14,17,20]. The possible effect of Mo on enhancing the coarsening resistance of TiC is often discussed according to the Ostwald's ripening theory:

$$r_f^3 - r_0^3 \propto C_{Ti} D_{Ti} \sigma_{\alpha/MC} \tag{9}$$

where r_f is the mean particle radius after aging, r_0 is the initial size, $\sigma_{\alpha/MC}$ is the interfacial energy of the MC/α interface, C_{Ti} is the equilibrium concentration of Ti in α matrix and D_{Ti} is the volume diffusivity. Fig. 11 shows the HR-TEM images of the nanosized carbide extracted from the 0Mo and 0.2Mo specimens after 16 h aging. The fast Fourier transformed diffractogram confirms that the precipitates in both steels have B1-type structure. By measuring the reciprocal of interplanar spacing of $(002)_{MC}$ (see the yellow line), the lattice constant of TiC and (Ti, Mo)C is estimated to be 0.438 nm and 0.424 nm, respectively, both of which are comparable to their reported values (TiC [23,57], (Ti, Mo)C [9,15]). Suppose that a_α=0.287 nm, the lattice misfit between TiC and α matrix is estimated to be 7.3% while that for (Ti, Mo)C is only 4.3%. Such a big drop indicates that Mo could reduce the interfacial energy of structural component effectively. Furthermore, as shown in **Supplementary material Fig. S3,** the chemical component of the (100) MC/α interface also decreases with increasing the Mo content in

[1] By using $\sigma_{\alpha/TiC} = 1.25$ J/m^2 and $\sigma_{\gamma/TiC} = 2.38$ J/m^2, r^* is estimated to be 0.47 nm, which is an acceptable value for carbide nucleation.

[2] The interfacial energy between BCC nucleus and α (or γ) remains unknown. We expect these values should be smaller or comparable with the chemical interfacial energy of B1-type nucleus. Therefore, the r^* for pure TiC cluster is estimated to be 0.24 nm by using $\sigma_{\alpha/TiC} = 0.339$ J/m^2 and $\sigma_{\gamma/MC} = 0.490$ J/m^2.

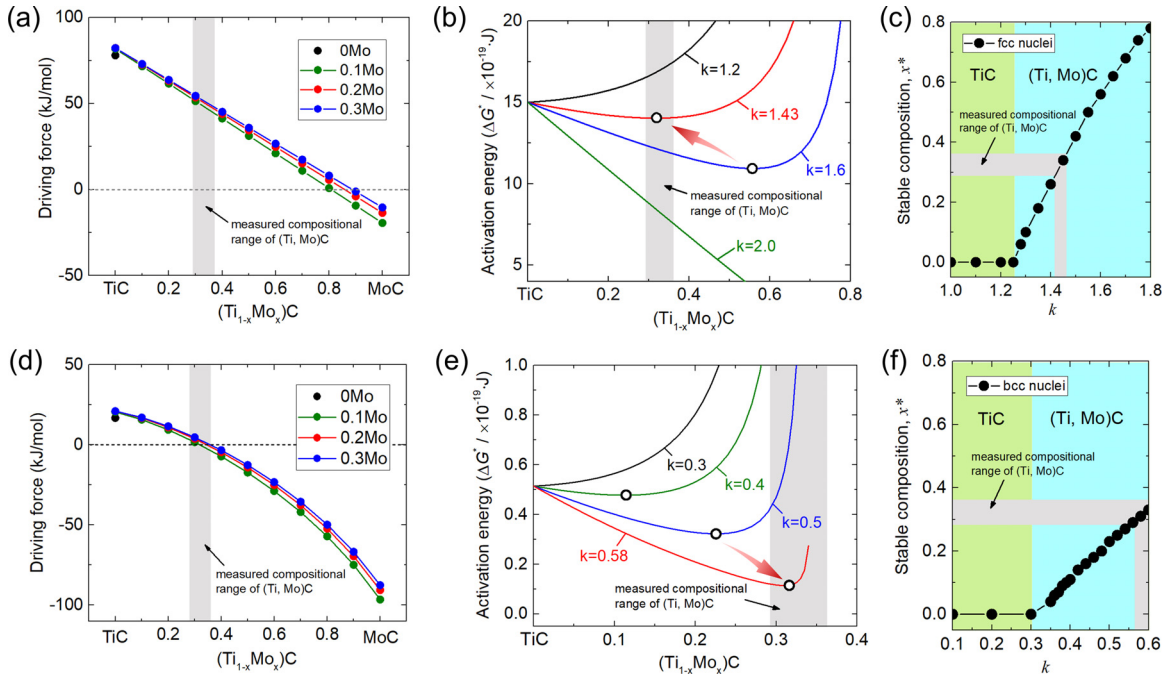

Fig. 10. (a,d) Calculated nucleation driving force and (b,e) activiation energy as a function of Mo site fraction (x) for (a,b) B1-type and (d,e) BCC-type nuclei at 660 °C. (c,f) plot the stable carbide compostion (x^*) against k values.

Table 2
Summary of the measured average Mo content in (Ti, Mo)C by different characterization techniques. The bulk composition of these materials is close to the current 0.2Mo alloy.

Ref.	[9]	[15]	[18]	[16]	[1]	Present study
Temperature, °C	680	650	650	650	Continuous cooling from 950 °C	660
Method	STEM-EDS	APT	SANS	APT	Chemical extraction	APT
Mo/(Ti+Mo), x	~34%	~30%	~25%	~33%	~46%	~29%

(Ti, Mo)C. Thus, one important reason for Mo addition to enhance the coarsening resistance of (Ti, Mo)C is lowering the interfacial energy of the MC/α interface both chemically and structurally.

On the other hand, by neglecting the term of r_0^3 in Eq. (9), the r_f^3 of the 0Mo alloy is estimated to be five times larger than that of the 0.2Mo alloy based on the experimental results (Fig. 9), which in other word suggests that $C_{Ti}D_{Ti}\sigma_{\alpha/MC}$ should be reduced five times by Mo addition. Such a large decrement, however, can hardly be explained by only considering the term of $\sigma_{\alpha/MC}$. In fact, the rate of carbide growth and coarsening are both controlled by solute diffusion in matrix near the MC/α interface, which at an atomic scale requires Ti atoms to overcome the diffusion energy barrier to attach to the MC. For simple MC precipitates, Ti diffusivity across the MC/α interface ($D_{Ti}^{trans.}$) is often assumed to be equal to the bulk diffusivity (D_{Ti}) in α. However, Mo partitioning into TiC could lead to the change of Ti activity across the MC/α interface and thus influence the trans-interface diffusivity of Ti via interaction between Mo and Ti atoms. In order to check whether such an interaction exists or not, first-principles calculations are subsequently performed.

Here, we simulated the migration behavior of Ti across the coherent interface between the BCC-α matrix and (Ti, Mo)C precipitates. Starting with the coherent TiC/α phase boundary with a dimension of 4.68 × 4.68 × 20.73 Å, the supercells containing (Ti, Mo)C/α phase boundaries can be constructed. Two scenarios, i.e. $Ti_{0.75}Mo_{0.25}C$ and $Ti_{0.5}Mo_{0.5}C$, with random substitution of Ti lattice sites by Mo are built by employing the similar local atomic environment method [58,59], which optimizes the atomic configurations through two-body and three-body correlation functions.

Fig. 12**(a–d)** describe the atomic arrangement of various atoms at the Fe-MC interfaces obeying the Baker-Nutting orientation relationship. At the interface, the C atoms located on the ocatahedral interstitial sites of (Ti,Mo)C correspond to the positions of Fe atoms in the BCC structure. The migration of Ti across the interface involves the formation of a vacancy at the interfacial layer of MC and movement of the vacancy towards the interfacial Fe layer. Fig. 12**(a)** shows an example that one substitutional Ti atom initially positioned in Fe (left figure), finally moves to the boundary of MC to form a complete MC layer (right figure). The total energy difference between the initial state and the transition state gives the migration energy. Indeed, the migration path is the shortest (~ 3.5 Å) one from Fe to MC phase, and is close to the jump distance for solute diffusion in α-Fe (~ 2.5 Å). Fig. 12**(d)** shows the profiles of diffusion energy of Ti across the α/MC interface. The activation enthalpy for self-diffusion of Ti (ΔH_m) corresponds to the energy peak with respect to zero. Clearly the ΔH_m increases with increasing Mo content in MC, which leads to an energy increment of 0.05 eV for $Ti_{0.75}Mo_{0.25}C$ and 0.20 eV for $Ti_{0.5}Mo_{0.5}C$. Such energy differences can yield $D_{Ti}^{trans.}$ being 2 to 13 times smaller than that in the Mo-free alloy, which gives a strong indication that Mo partitioning into TiC also plays a significant role in the local Ti diffusivity near the (Ti, Mo)C/α interface and thus the coarsening rate. The physical origin lies in the repulsive interaction between Ti and Mo atoms, which is expected to be applicable to other multi-alloying systems like V-Mo and Nb-Mo.

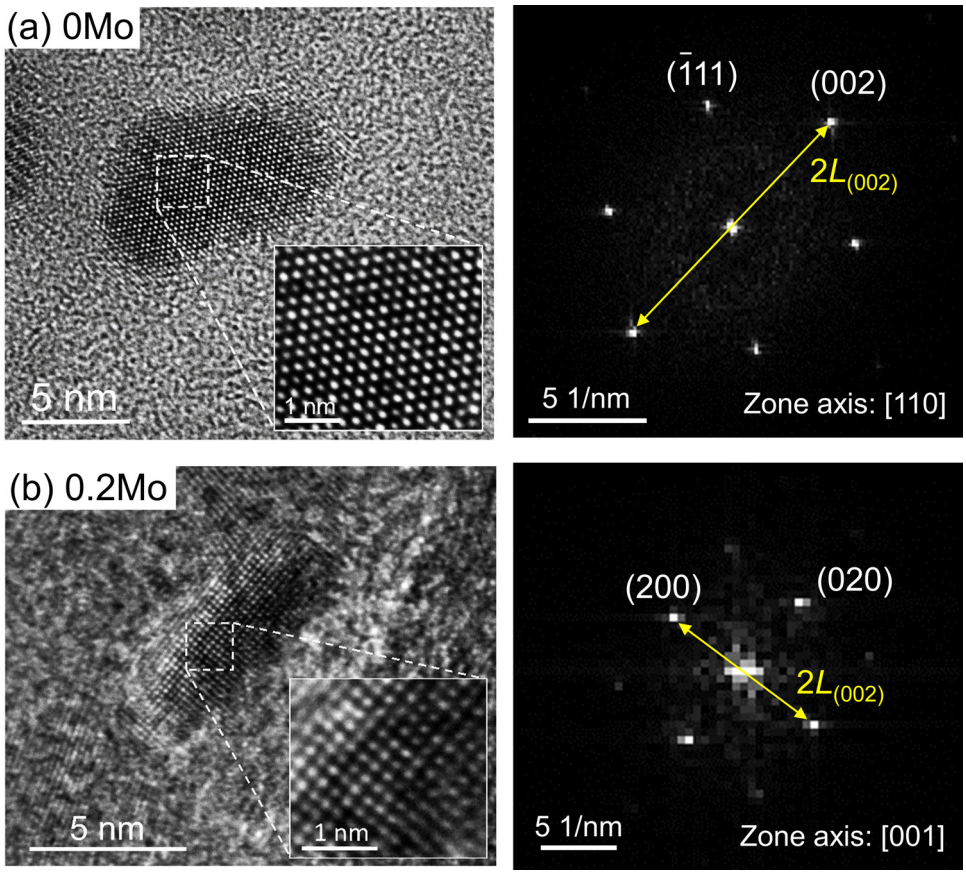

Fig. 11. HR-TEM, fast Fourier transformed diffractogram (FFT) and inverse fast Fourier transformed diffractogram (IFFT) images of nanosized carbide extracted from the (a) 0Mo and (b) 0.2Mo specimens after 16 h aging (For interpretation of the references to color in this figure, the reader is referred to the web version of this article).

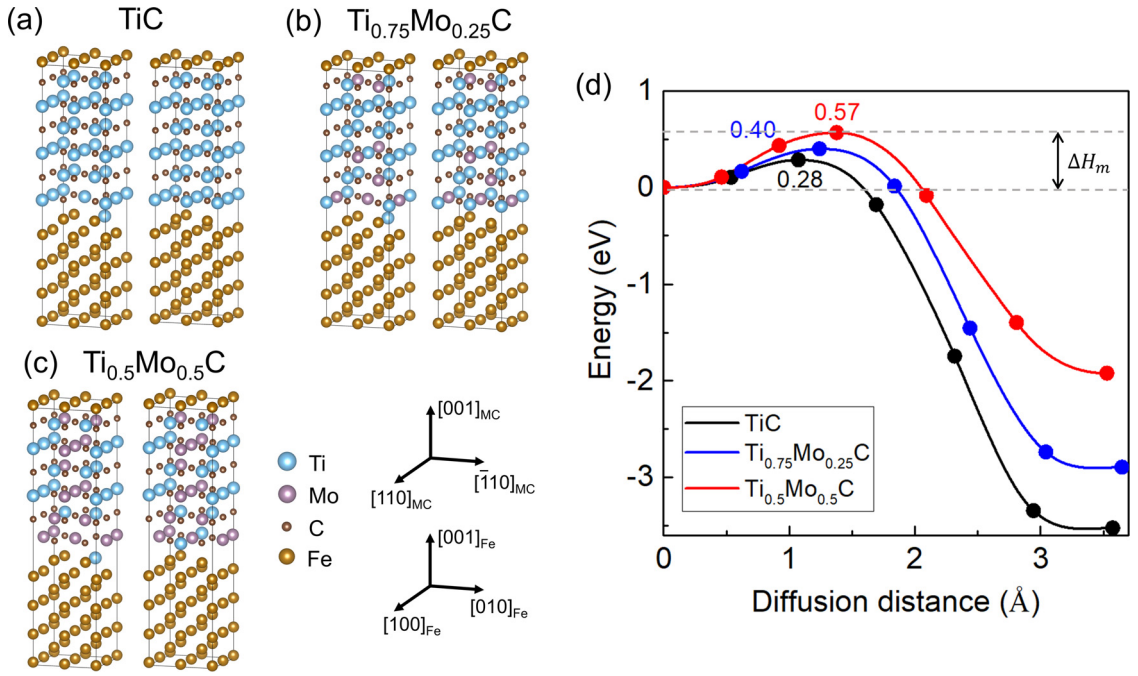

Fig. 12. Structures and CINEB results for simulating Ti diffusion from α matrix to MC carbide with different composition: (a) TiC, (b) $Ti_{0.75}Mo_{0.25}C$, (c) $Ti_{0.5}Mo_{0.5}C$. (d) Diffusion energy profiles of Ti across the α/MC interface. The structures in (a)–(c) at left side and right side represent the atomic configurations before and after diffusion.

5. Conclusion

In this study, the interphase precipitation behavior in Ti-Mo-bearing low carbon steels was systematically studied by combining the multi-scale characterizations and theoretical analysis. It was interestingly found that the average site fraction of Mo in (Ti, Mo)C was almost independent on the bulk Mo content. Compared to the Mo-free alloy, the number density of interphase precipitates was substantially enhanced by Mo addition, while it can hardly be enhanced via further increasing the bulk Mo content. The number density is intrinsically controlled by the fraction of Mo in (Ti, Mo)C, which competitively influences the driving force for (Ti, Mo)C nucleation and the interfacial energy of the (Ti, Mo)C/α and (Ti, Mo)C/γ interfaces. The coarsening resistance of interphase precipitates can be notably improved by Mo addition ($>$ 0.1mass%) that reduces both the interfacial energy and Ti trans-interface diffusivity.

Declaration of Competing Interest

The authors declare that they have no known competing financial interests or personal relationships that could have appeared to influence the work reported in this paper.

Acknowledgments

H. -K. Dong and Z. -G. Yang acknowledges financial support from the National Natural Science Foundation of China (grants 5217010323, 51771100). H. Chen acknowledges financial support from the National Natural Science Foundation of China (grants 51922054, U1764252, U1860109 and U1808208). A. Riyahi khorasgani and T. Li would like to thank Zentrum für Grenzflächendominierte Höchstleistungswerkstoffe (ZGH) at Ruhr University Bochum for the access to infrastructure (LEAP 5000XR and FEI Helios G4 CX FIB/SEM).

Supplementary materials

Supplementary material associated with this article can be found, in the online version, at doi:10.1016/j.actamat.2021.117475.

References

[1] Y. Funakawa, T. Shiozaki, K. Tomita, T. Yamamoto, E. Maeda, Development of high strength hot-rolled sheet steel consisting of ferrite and nanometer-sized carbides, ISIJ Int. 44 (2004) 1945–1951.
[2] K. Seto, Y. Funakawa, S. Kaneko, Hot rolled high strength steels for suspension and chassis parts “NANOHITEN” and “BHT steel, JFE Tech. Rep. 10 (2007) 19–25.
[3] A.T. Davenport, R.W.K. Honeycombe, Precipitation of carbides at $\gamma \rightarrow \alpha$ boundaries in alloy steels, Proc. R. Soc. Lond. A 322 (1971) 191–205.
[4] R.W.K. Honeycombe, R.F. Mehl, Transformation from austenite in alloy steels, Metall. Trans. A 7 (1976) 915–936.
[5] W.B Lee, S.G Hong, C.G Park, K.H Kim, S.H Park, Influence of Mo on precipitation hardening in hot rolled HSLA steels containing Nb, Scr. Mater. 43 (2000) 319–324.
[6] J.H. Jang, Y.U. Heo, C.H. Lee, H.K.D.H. Bhadeshia, DW Suh, Interphase precipitation in Ti–Nb and Ti–Nb–Mo bearing steel, Mater. Sci. Technol. 29 (2014) 309–313.
[7] J.B. Seol, S.H. Na, B. Gault, J.C. Han, C.G. Park, D. Raabe, Core-shell nanoparticle arrays double the strength of steel, Sci. Rep. 7 (2017) 1–9.
[8] P. Gong, X.G. Liu, A. Rijkenberg, W.M. Rainforth, The effect of molybdenum on interphase precipitation and microstructures in microalloyed steels containing titanium and vanadium, Acta Mater. 161 (2018) 374–387.
[9] H.W. Yen, C.Y. Huang, J.R. Yang, Characterization of interphase-precipitated nanometer-sized carbides in a Ti–Mo-bearing steel, Scr. Mater. 61 (2009) 616–619.
[10] H.W. Yen, P.Y. Chen, C.Y. Huang, J.R. Yang, Interphase precipitation of nanometer-sized carbides in a titanium–molybdenum-bearing low-carbon steel, Acta Mater. 59 (2011) 6264–6274.
[11] C.Y. Chen, H.W. Yen, F.H. Kao, W.C. Li, C.Y. Huang, J.R. Yang, Precipitation hardening of high-strength low-alloy steels by nanometer-sized carbides, Mater. Sci. Eng. A 499 (2009) 162–166.
[12] Z.Q. Wang, X.J. Sun, Z.G. Yang, Q.L. Yong, C. Zhang, Z.D. Li, Y.Q. Weng, Carbide precipitation in austenite of a Ti–Mo-containing low-carbon steel during stress relaxation, Mater. Sci. Eng. A 573 (2013) 84–91.
[13] S. Mukherjee, I.B. Timokhina, C. Zhu, S.P. Ringer, P.D. Hodgson, Three-dimensional atom probe microscopy study of interphase precipitation and nanoclusters in thermomechanically treated titanium–molybdenum steels, Acta Mater. 61 (2013) 2521–2530.
[14] N. Kamikawa, Y. Abe, G. Miyamoto, Y. Funakawa, T. Furuhara, Tensile behavior of Ti, Mo-added low carbon steels with interphase precipitation, ISIJ Int. 54 (2014) 212–221.
[15] J. Wang, M. Weyland, I. Bikmukhametov, M.K. Miller, P.D. Hodgson, I. Timokhina, Transformation from cluster to nano-precipitate in microalloyed ferritic steel, Scr. Mater. 160 (2019) 53–57.
[16] J. Wang, P.D. Hodgson, I. Bikmukhametov, M.K. Miller, I. Timokhina, Effects of hot-deformation on grain boundary precipitation and segregation in Ti-Mo microalloyed steels, Mater. Des. 141 (2018) 48–56.
[17] J.H. Jang, C.H. Lee, Y.U. Heo, D.W. Suh, Stability of (Ti, M)C (M=Nb, V, Mo and W) carbide in steels using first-principles calculations, Acta Mater. 60 (2012) 208–217.
[18] Y.Q. Wang, S. Sridhar, P.D. Lee, S.J. Clark, B. Cai, D. AlbaVenero, K. Yun, M. Gorley, E. Surrey, D.G. McCartney, S. Sridhar, P.D. Lee, Small-angle neutron scattering reveals the effect of Mo on interphase nano-precipitation in Ti-Mo micro-alloyed steels, Scr. Mater. 174 (2020) 24–28.
[19] Z.Q. Wang, H. Chen, Z.G. Yang, F.C. Jiang, Decelerated coarsening of (Ti, Mo)C particles with a core–shell structure in austenite of a Ti-Mo-bearing steel, Metall. Mater. Trans. A 49 (2018) 1455–1459.
[20] Y. Funakawa, K. Seto, Coarsening behavior of nanometer-sized carbides in hot-rolled high strength sheet steel, Mater. Sci. Forum 539 (2007) 4813–4818.
[21] D. Vaumousse, A. Cerezo, P.J. Warren, A procedure for quantification of precipitate microstructures from three-dimensional atom probe data, Ultramicroscopy 95 (2003) 215–221.
[22] B. Gault, F. Danoix, K. Hoummada, D. Mangelinck, H. Leitner, Impact of directional walk on atom probe microanalysis, Ultramicroscopy 113 (2012) 182–191.
[23] A. Nartowski, I. Parkin, M. MacKenzie, A. Craven, I. MacLeod, Solid state metathesis routes to transition metal carbides, J. Mater. Chem. 9 (1999) 1275–1281.
[24] G. Kresse, J. Furthmuller, Efficient iterative schemes for ab initio total-energy calculations using a plane-wave basis set, Phys. Rev. B 54 (1996) 11169–11186.
[25] P.E. Blöchl, Projector augmented-wave method, Phys. Rev. B 50 (1994) 17953–17979.
[26] G. Kresse, D. Joubert, From ultrasoft pseudopotentials to the projector augmented-wave method, Phys. Rev. B 59 (1999) 1758–1775.
[27] J.P. Perdew, J.A. Chevary, S.H. Vosko, K.A. Jackson, M.R. Pederson, D.J. Singh, C. Fiolhais, Atoms, molecules, solids, and surfaces: Applications of the generalized gradient approximation for exchange and correlation, Phys. Rev. B 46 (1992) 6671–6687.
[28] J.P. Perdew, K. Burke, M. Ernzerhof, Generalized gradient approximation made simple, Phys. Rev. Lett. 77 (1996) 3865–3868.
[29] M. Methfessel, A.T. Paxton, High-precision sampling for Brillouin-zone integration in metals, Phys. Rev. B Condens. Matter 40 (1989) 3616–3621.
[30] G. Henkelman, B.P. Uberuaga, H. Jónsson, A climbing image nudged elastic band method for finding saddle points and minimum energy paths, J. Chem. Phys. 113 (2000) 9901–9904.
[31] M. Enomoto, H.I. Aaronson, Nucleation kinetics of proeutectoid ferrite at austenite grain boundaries in Fe-C-X alloys, Metall. Trans. A 17 (1986) 1385–1397.
[32] C. Hutchinson, H. Zurob, Y. Brechet, The growth of ferrite in Fe-C-X alloys: the role of \dynamics, diffusion, and interfacial conditions, Metall. Mater. Trans. A 37 (2006) 1711–1720.
[33] G. Miyamoto, K. Yokoyama, T. Furuhara, Quantitative analysis of Mo solute drag effect on ferrite and bainite transformations in Fe-0.4C-0.5Mo alloy, Acta Mater. 177 (2019) 187–197.
[34] T. Sakuma, R.W.K. Honeycombe, Microstructures of isothermally transformed Fe-Nb-C alloys, Met. Sci. 18 (1984) 449–454.
[35] R. Lagneborg, S. Zajac, A model for interphase precipitation in V-microalloyed structural steels, Metall. Mater. Trans. A 32 (2001) 39–50.
[36] T. Murakami, H. Hatano, G. Miyamoto, T. Furuhara, Effects of ferrite growth rate on interphase boundary precipitation in V microalloyed steels, ISIJ Int. 52 (2012) 616–625.
[37] A.T.W. Kempen, F. Sommer, E.J. Mittemeijer, The kinetics of the austenite-ferrite phase transformation of Fe-Mn: differential thermal analysis during cooling, Acta Mater. 50 (2002) 3545–3555.
[38] A.J. Breen, K.Y. Xie, M.P. Moody, B. Gault, H.W. Yen, C.C. Wong, J.M. Cairney, S.P. Ringer, Resolving the morphology of niobium carbonitride nano-precipitates in steel using atom probe tomography, Microsc. Microanal. 20 (2014) 1100–1110.
[39] R.P. Kolli, D.N. Seidman, Co-precipitated and collocated carbides and Cu-Rich precipitates in a Fe-Cu steel characterized by atom-probe tomography, Micros. Microanal. 20 (2014) 1727–1739.
[40] M.K. Miller, M.G. Hetherington, Local magnification effects in the atom probe, Surf. Sci. 246 (1991) 442–449.
[41] M. Thuvanderm, J. Weidow, J. Angseryd, L.K.L. Falk, F. Liu, M. Sonestedt, K. Stiller, H.O. Andren, Quantitative atom probe analysis of carbides, Ultramicroscopy 111 (2011) 604–608.

[42] Y.J. Zhang, G. Miyamoto, K. Shinbo, T. Furuhara, Effects of α/γ orientation relationship on VC interphase precipitation in low-carbon steels, Scr. Mater. 69 (2013) 17–20.
[43] Y.J. Zhang, G. Miyamoto, K. Shinbo, T. Furuhara, T. Ohmura, T. Suzuki, K. Tsuzaki, Effects of transformation temperature on VC interphase precipitation and resultant hardness in low-carbon steels, Acta Mater. 84 (2015) 375–384.
[44] M. Enomoto, in: Phase Transformation in Metals: Introduction to the Science of Materials Microstructure, Uchida Rokakuho, Tokyo, 2000, p. 40.
[45] H.K.D.H. Bhadeshia, Diffusional transformations: a theory for the formation of superledges, Phys. Status Solidi A Appl. Res. 69 (1982) 745–750.
[46] J.M. Howe, in: Interfaces in Materials: Atomic Structure, Thermodynamics and Kinetics of Solid-Vapor, Solid-Liquid and Solid-Solid Interfaces, Wiley-Interscience, NY, 1997, p. 378.
[47] K.C. Russell, Nucleation in solids: the induction and steady state effects, Adv. Colloid Interface 13 (1980) 205–318.
[48] J. Fridberg, L.E. Torndahl, M. Hillert, Diffusion in iron, Jernkontorets Ann 153 (1969) 263–276.
[49] Y.J. Zhang, G. Miyamoto, K. Shinbo, T. Furuhara, Quantitative measurements of phase equilibria at migrating α/γ interface and dispersion of VC interphase precipitates: evaluation of driving force for interphase precipitation, Acta Mater. 128 (2017) 166–175.
[50] W.S. Jung, S.C. Lee, S.H. Chung, Energetics for interfaces between group IV transition metal carbides and bcc iron, ISIJ Int. 48 (2008) 1280–1284.
[51] N.Y. Park, J.H. Choi, P.R. Cha, W.S. Jung, S.H. Chung, S.C. Lee, First-principles study of the interfaces between Fe and transition metal carbides, J. Phys. Chem. A 117 (2012) 187–193.
[52] Z.Q. Wang, H. Zhang, C.H. Guo, W.L. Liu, Z.G. Yang, X.J. Sun, Z.Y. Zhang, F.C. Jiang, Effect of molybdenum addition on the precipitation of carbides in the austenite matrix of titanium micro-alloyed steels, J. Mater. Sci. 51 (2016) 4996–5007.
[53] Z.G. Yang, M. Enomoto, Discrete lattice plane analysis of Baker–Nutting related B1 compound/ferrite interfacial energy, Mater. Sci. Eng. A 332 (2002) 184–192.
[54] Z.G. Yang, M. Enomoto, Calculation of the interfacial energy of B1-type carbides and nitrides with austenite, Metall. Mater. Trans. A 32 (2001) 267–274.
[55] D.H.R. Fors, G. Wahnström, Theoretical study of interface structure and energetics in semicoherent Fe(001)/MX(001) systems (M=Sc, Ti, V, Cr, Zr, Nb, Hf, Ta; X=C or N), Phys. Rev. B 82 (2010) 195410.
[56] H.C. Wang, Y.J. Li, E. Detemple, G. Eggeler, Revealing the two-step nucleation and growth mechanism of vanadium carbonitrides in microalloyed steels, Scr. Mater. 187 (2020) 350–354.
[57] J.C. Grossman, A. Mizel, M. Cote, M.L. Cohen, S.G. Louie, Transition metals and their carbides and nitrides: trends in electronic and structural properties, Phys. Rev. B 60 (1999) 6343–6347.
[58] H.Q. Song, F.Y. Tian, Q.M. Hu, L. Vitos, Y.D. Wang, J. Shen, N.X. Chen, Local lattice distortion in high-entropy alloys, Phys. Rev. Mater. 1 (2017) 023404.
[59] F. Tian, D.Y. Lin, X. Gao, H. Song, Y.F. Zhao, H. Song, A structural modeling approach to the solid-solution materials, J. Chem. Phys. 153 (2020) 034101.